Article

Segmented Highly Reversible Thermochromic Layered Perovskite [(CH₂)₂(NH₃)₂]CuCl₄ Crystal Coupled with an Inverse Magnetocaloric Effect

Somrita Dutta, Deepak Vishnu S. K, Sudipta Som, Rajneesh Chaurasiya, Dinesh Kumar Patel, Kalimuthu Moovendaran, Cheng-Chieh Lin, Chun-Wei Chen,* and Raman Sankar*

Read Online

ACCESS | Metrics & More | Article Recommendations | Supporting Information

ABSTRACT: The layered, lead-free hybrid perovskites are superior in organic electronics compared to their three-dimensional (3D) counterparts due to their facile synthesis and promising stability to various environmental conditions. To learn more about the multifunctional side of such materials, a layered perovskite (EDA)CuCl₄ [EDA is (CH₂)₂(NH₃)₂] crystal was grown in solution and crystallographically characterized by single-crystal X-ray diffraction. The crystal is thermally very stable and exhibits a high reversible thermochromic working temperature (∼503 K), intense conductivity changes with temperature, and strong exotic magnetic properties. The structural changes of the crystal with temperature are monitored and explained by powder X-ray diffraction and UV−vis absorption. The absorption band of the crystal shows little variation after repeated heating/cooling cycles, indicating admirable stability. Moreover, the Cu hybrid consists of a strong ferromagnetic interaction in antiferromagnetically coupled layers with a Néel temperature of about 34 K. The magnetocaloric effect of the crystal was investigated and found to be inverse due to the magnetic entropy change associated with the antiferromagnetic transition and the strong ferromagnetic interaction, indicating the suitability of the perovskite hybrid as a candidate for an environmentally friendly low-temperature magnetic cooling technology. The overall results promise a potential multipurpose two-dimensional (2D) perovskite for future electronic applications in a wide temperature range.

KEYWORDS: 2D perovskite, single crystal, thermochromism, magnetocaloric effect, antiferromagnetism
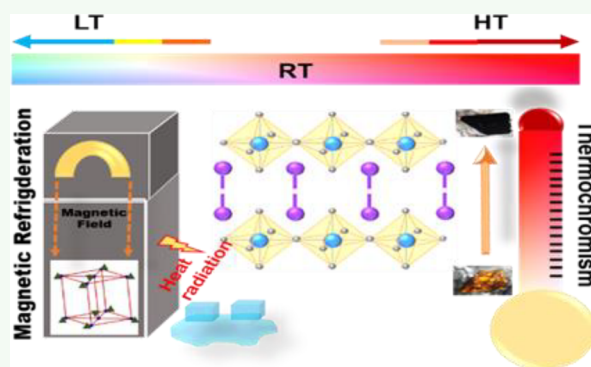
INTRODUCTION

The versatile and promising properties of organic−inorganic hybrid perovskites (OIHP), or simply HPs, have attracted the attention of materials researchers around the world and brought them to the forefront of the organic semiconductor industry. This renaissance of OIHPs, initiated by CH₃NH₃PbI₃, has been noticed by their application in high photovoltaics emanating from their outstanding properties.[1−4] Nevertheless, the limitations related to structural engineering in the three-dimensional (3D) perovskites led to the reduction of dimensionality with the realization of various layered two-dimensional (2D) HPs. The layered 2D perovskites consist of multiple quantum well (MQW) structures with the organic molecular layers acting as potential barriers separating infinite inorganic layers with angular octahedra acting as the potential wells[5] and can combine the brilliant properties of their organic and the inorganic components. The organic part, with its lower dielectric constant and wide band gap, gives the hybrids flexibility, softness, and structural diversity, while the inorganic components help regulate various properties, including optical,

electrical, and magnetic properties, along with their hardness and thermal stability.[6−8] Due to this structural softness and stability, the structure can be easily reshaped under external influences such as heat, light, electricity, magnetism, etc., resulting in a series of phase transitions. This set of unique properties, along with the ability to chemically tune the metal and halide ions and the flexibility to incorporate organic cations into their structure, has carved out a unique research niche for the development of functional materials for optoelectronics, magnetism, spintronics, and smart materials.[9−14] The (100)-oriented 2D lead (Pb²⁺)-based 2D HPs, conceptually obtained by slicing the 3D perovskite structure along the (100) plane, is the most widely studied HP for
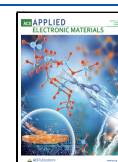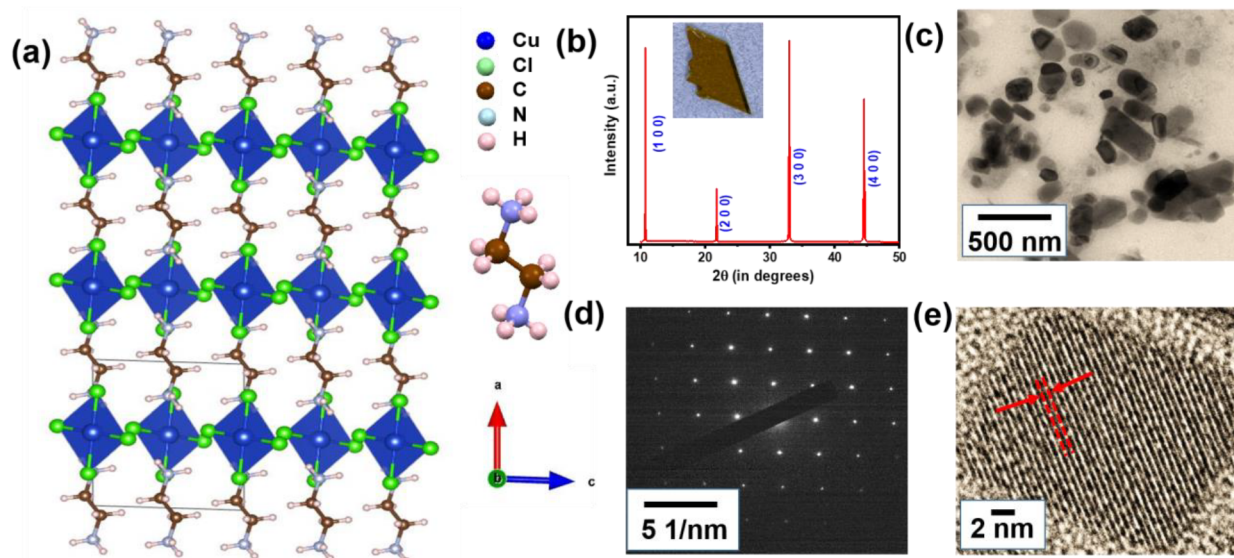
Figure 1. (a) Layered structure of (EDA)CuCl$_4$ along the *a* direction; inset, the molecular structure of EDA. (b) XRD of the single crystal with a photo in the inset. (c) TEM, (d) SAED pattern, and (e) HRTEM of the 2D perovskite

various optoelectronic applications.[15−18] Due to the toxicity issues of Pb^{2+}, alternative divalent ions have been proposed as a replacement.[19−21] Copper (Cu^{2+}), compared to other ions, is a readily available transition metal element that is less likely to oxidize in ambient atmospheres and, due to its smaller effective ionic radius (73 pm), inhibits the formation of a 3D perovskite, thus conferring a very stable 2D structure. In addition, Cu compounds exhibit a strong Jahn−Teller distortion in the [MX$_6$] octahedra, leading to a highly flexible structure and allowing great tunability by external influences.[22,23] Copper-based HPs have been predominantly considered mainly for their magnetic properties,[24−28] but they have also been considered as likely Pb-free perovskite candidates for other applications.[29−32] With the existence of an abundance of 2D HPs, many materials are available in the literature that have provided fundamental studies from one or two perspectives. Since such materials offer great scope for new targets, we have here reexamined one such copper-based layered perovskite (EDA)CuCl$_4$ (EDA is ethylenediamine). The crystal, first reported in 1972, is studied for its structural, magnetic, and optical properties and also the effects with the increase in the organic chain length of this series of hybrid.[33−40] Since the earlier reports provided some unique insights, in our current work we have tried to explore the applicability aspect of the material by investigating two very different properties of the perovskite—thermochromism and the magnetocaloric effect (MCE).

Thermochromism is the color change of any material with a change in temperature caused by geometric changes in the lattice structure. Copper hybrids containing CuCl$_4$$^{2−}$ are usually thermochromic because the hydrogen bonds of the cation change in response to temperature, causing the geometry of the [CuCl$_4$]$^{2−}$ anion to change from a square plane to a tetrahedral one, resulting in a color change.[41] However, due to their thermal instability, low thermochromic temperatures are reported for 2D HPs.[42] In the present work, we investigate the temperature-dependent structural and optical properties of the (EDA)CuCl$_4$ crystal to reveal its exotic thermochromic behavior, which makes it a potential candidate for smart windows, thermal sensors, and so on. On

the other hand, the MCE is based on the changes of adiabatic temperature and isothermal magnetic entropy in materials when an external magnetic field is applied. Materials which are mostly based on rare earths and have high a MCE are environmentally friendly and cost-effective and can be used in cooling technology.[43−46] The normal or conventional MCE (CMCE) concerns the decrease in magnetic entropy caused by adiabatic demagnetization when a material is exposed to a magnetic field. Inverse magnetic configurational entropy (IMCE) is another possibility when a material is exposed to magnetic fields which are cooled by adiabatic magnetization. Therefore, these materials can serve as heat sinks and can be used as composites with conventional refrigerants to improve cooling efficiency.[47] In the literature, there are a few works on the MCE in 2D HP, which reveal their promising results as magnetocaloric materials.[48−50] In the current report, we have re-examined the magnetic properties of the (EDA)CuCl$_4$ perovskite. Moreover, we explore the caloric effect due to magnetism (MCE) and show its potential use in low-temperature magnetic cooling.

Despite extensive research on 2D HPs, these two above properties are never reported together because they are mutually exclusive. However, since thermochromism is observed upon heating and MCE applies to cooling at low temperatures, a single material showing good results for both properties can provide a wide temperature window for application. Therefore, we decided to report these two properties together. This work could show a potential way for integrating multiple stimuli into single 2D hybrid perovskites with easy-to-make methods and logical control functions, thus expanding their applications as multifunctional materials.

■ MATERIALS AND METHODS

(EDA)CuCl$_4$ single crystals were synthesized from a stoichiometric solution of cupric chloride and ethylenediammonium powders in water following its slow evaporation at ambient conditions. Golden-yellow single crystals, which grow layer by layer alongside the [100] direction, were obtained after a few days.
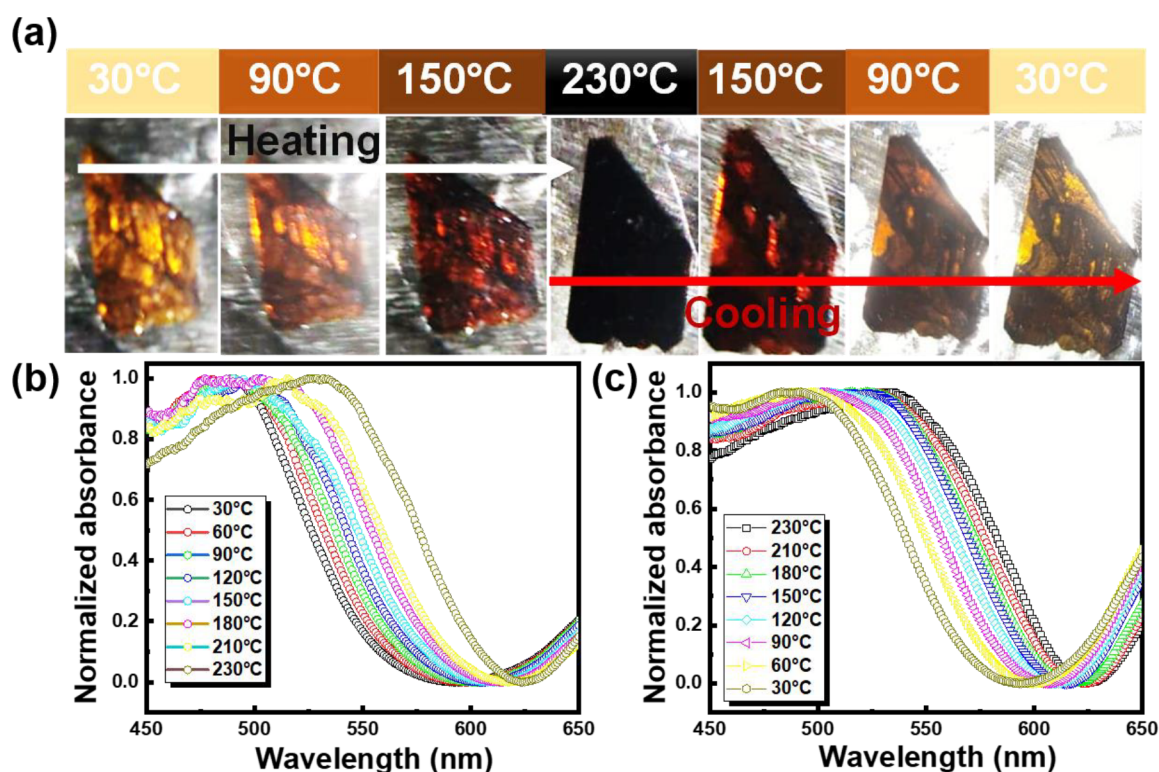
Figure 2. (a) Optical micrograph of the crystal with temperature variation. Change of absorbance with (b) increasing temperature and (c) decreasing temperature.

Single-crystal X-ray diffraction (SCXRD) was utilized to redetermine the crystal structure and to obtain precise values for bond lengths and angles within the $[CuCl_4]^{2-}$ ion and intermolecular interactions. The structural analysis of the achieved powders was characterized by a Bruker D8 Focus powder X-ray diffractometer. The obtained results were further used for Rietveld refinement to verify the structure and the growth direction of the crystal. The thermal analysis of the single crystal was checked by an SDT 650 thermogravimetric differential scanning calorimeter analyzer (TG DSC). The UV−vis spectra were recorded with a UV−vis spectrophotometer (BRIC 1200). The electrical measurement data was collected with a Keithley 2400. A superconducting quantum interference device−vibrating sample magnetometer (SQUID−VSM, Quantum Design, U.S.A.) was used to measure the magnetic behavior of the single crystals. The data for the specific heat was achieved with a physical property measurement system (PPMS, Quantum Design, U.S.A.) using a standard relaxation method.

Computational Details. The structural, electronic, and magnetic properties of $(EDA)CuCl_4$ were investigated using the density functional theory (DFT)-based Quantum ESPRESSO (QE) package.[51] Initial structural information was taken from our experimental data. Further, the crystal structure was optimized by minimizing the force on each atom and the energy of the supercell. The generalized gradient approximation of Perdew−Burke−Ernzerhof (GGA-PBE) was used as an exchange-correlation functional.[52] Ultrasoft pseudopotentials were used to define the potential of core and semicore electrons. The kinetic energy cutoff for the wave function was considered to be 650 eV throughout the calculation. The self-consistent energy cutoff convergence criteria were set to 1×10^{-7} eV. The force and energy cutoff for optimizing the crystal structure were fixed to 0.02 eV/Å and 1×10^{-3} eV, respectively. The sampling of the Brillouin zone was carried out using $2 \times 2 \times 1$ k-points under the Monkhorst−Pack scheme.[53] Further, we have created a $2 \times 2 \times 1$ supercell to consider the different spin conditions for ferromagnetic and antiferromagnetic states. The stability of different magnetic states was investigated in terms of total energy.

RESULTS AND DISCUSSION

Structure Analysis. The SCXRD data reveal the layered structure of the $(EDA)CuCl_4$ perovskite shown in Figure 1a, which consists of inorganic layers of distorted square-planar $[CuCl_4]^{2-}$ ions due to the Jahn−Teller effect, with the organic diammonium EDA (cation in Figure 1) connecting the layers. The crystallographic parameters are briefly presented in Tables S1 and S2. The results obtained are in a similar order to the previous studies.[32,33] Figure 1b shows the excellent crystallinity of the $(EDA)CuCl_4$ single crystal with peaks that can be indexed as ($h00$) reflections in agreement with the monoclinic $P21/c$ (no. 14) space group and also show the growth of the crystal parallel to the a-axis. The phase purity of the powdered single crystals was investigated by powder X-ray fluorescence (PXRD) analysis, which agreed with the simulated structure obtained from the single crystal structure (Figure S1) and confirmed the phase purity of the diammonium salt. To investigate the structural alignment and chemical purity of the synthesized $(EDA)CuCl_4$ single crystal, transmission electron microscopy (TEM) analysis is performed. The TEM image of the $(EDA)CuCl_4$ single crystal is shown in Figure 1c. The selected area diffraction pattern (SAED) and the high-resolution transmission images (HRTEM) of the $(EDA)CuCl_4$ single crystal show the presence of planes along the (100) directions as shown in Figure 1, parts d and e, respectively. The diffraction spots are strong along the (100) direction, confirming the formation of a high-quality $(EDA)CuCl_4$ single crystal.

Thermogravimetric measurements (TG DSC) are performed to verify the thermal stability of the crystals. A decomposition temperature of about 503 K (Figure S2) is obtained, demonstrating the high thermal stability of the Cu-based crystal. We then investigated the variations in the optical
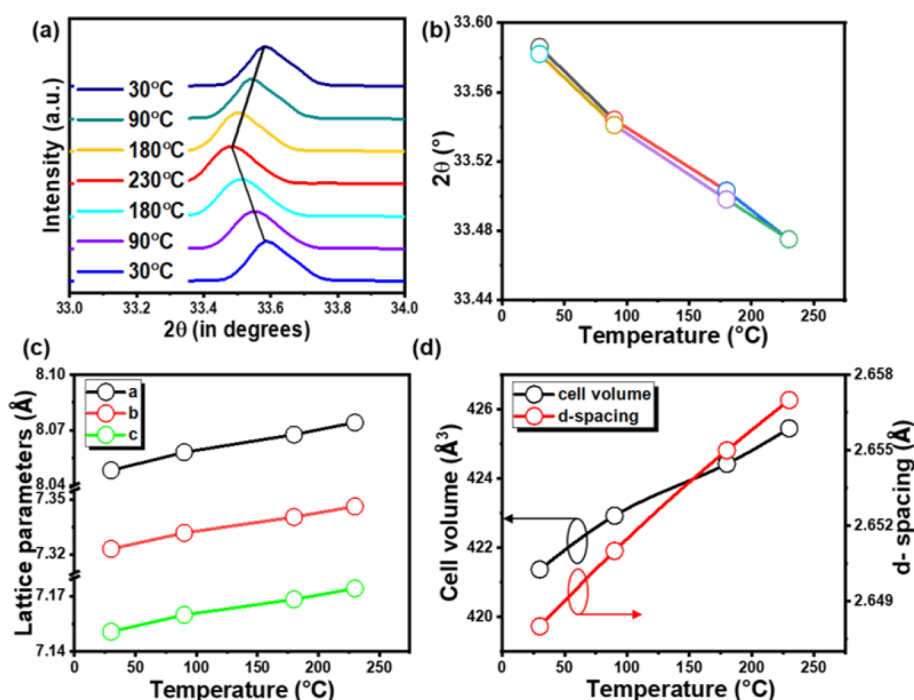
Figure 3. (a) XRD peak shift with temperature variation. (b) Change of 2θ with increasing and decreasing temperature. (c) Temperature variation of the (c) lattice parameters and (d) interplanar spacing and cell volume.

properties of the single crystal from room temperature (RT) to 230 °C (503 K). The experiment was carried out in ambient conditions. The optical image changes with temperature are shown in Figure 2a. An obvious thermochromic phenomenon with increasing temperature is observed. At room temperature, the $(EDA)CuCl_4$ crystal exhibits a golden-yellow color, which slowly changes to an almost black color as the temperature increases. However, the exciting thing is that the single crystal (SC) returns to its original color when cooled to RT, indicating the reversible thermochromism of the 2D perovskite. The absorption spectra of the SC upon heating and cooling are shown in Figure 2, parts b and c, respectively. With the increase of temperature from RT to 230 °C, the edge of the absorption band shows a steady shift toward higher wavelengths, indicating the narrowing of the band gap for the SC, while the reverse effect is observed upon cooling.

The change in the band gap with temperature variations from 30 to 230 °C is shown in Figure S3. The decrease in the band gap is consistent with the darkening of the crystal color with increasing temperature. To confirm the stability of the samples, the absorption spectra were measured repeatedly for heating/cooling cycles (Figure S4). This shows an insignificant deterioration of the single crystal within the mentioned temperature range (30−230 °C). To investigate the fluctuations in the crystal structure, temperature-dependent PXRD patterns of the powdered crystal are recorded by heating it from RT to 230 °C, and then cooling it back to 30 °C. Figure 3a shows the diffraction peak at $2\theta = 33.59°$, which shifts to lower 2θ angles when the temperature is increased ($2\theta = 33.46°$ at 230 °C) and finally moves back to the higher 2θ value when cooled. The reversible change in the 2θ angle is illustrated in Figure 3b, which shows a very small hysteresis also observed in some other 2D crystals.[54,55]

The structural change of the crystal upon heating is shown in Figure 3, parts c and d, by observing the lattice parameters (a, b, and c), the lattice spacing parameter d, and the changes

in lattice volume with increasing temperature, which illustrates the standard lattice expansion within the crystal with increasing temperature. The gradual lattice expansion is also consistent with the DSC measurements, which show no thermal irregularities in the temperature range of RT−503 K (Figure S2). The lattice constant leads to an increase in the distance between the electron clouds of two interacting atoms and thus leads to a decrease in the binding force between the valence electrons and a decrease in the binding energy of the parent atoms.[56] A decrease in binding energy means a decrease in the band gap, which causes the color change of the crystals. On cooling, the binding energy increases again due to lattice contraction, and the color of the SC recovers. Therefore, the thermally induced lattice expansion is the only cause that gives rise to the excellent reversible thermochromism without phase change of the 2D crystal structure.

The current−voltage ($I−V$) characteristics of the perovskite from room temperature to its decomposition temperature were plotted and are shown in Figure 4. The linearity of the $I−V$ curves proves that the contact between the electrodes and the material is ohmic. The value of conductivity increases significantly with temperature, which confirms the semiconductor behavior of the perovskite. It is also found that the change in conductivity with temperature variation is reversible. The highest value of electrical conductivity of $(EDA)CuCl_4$ is 7.03×10^{-11} S/cm at 503 K and decreases to 3.33×10^{-16} S/cm at 303 K or RT. In a recent report, Sun et al.[54] reported excellent reversible thermochromism in $(BED)_2CuCl_6$ at a working temperature of 443 K. This is the highest temperature to date for a 2D hybrid material with a very high order of magnitude dependence of conductivity on temperature. When compared to $(BED)_2CuCl_6$, our material, $(EDA)CuCl_4$, has a high thermochromic working temperature of 230 °C (503 K), as well as a conductivity change of about 5 orders of magnitude with a reversible tendency with temperature. The excellent reversibility of color and significant change
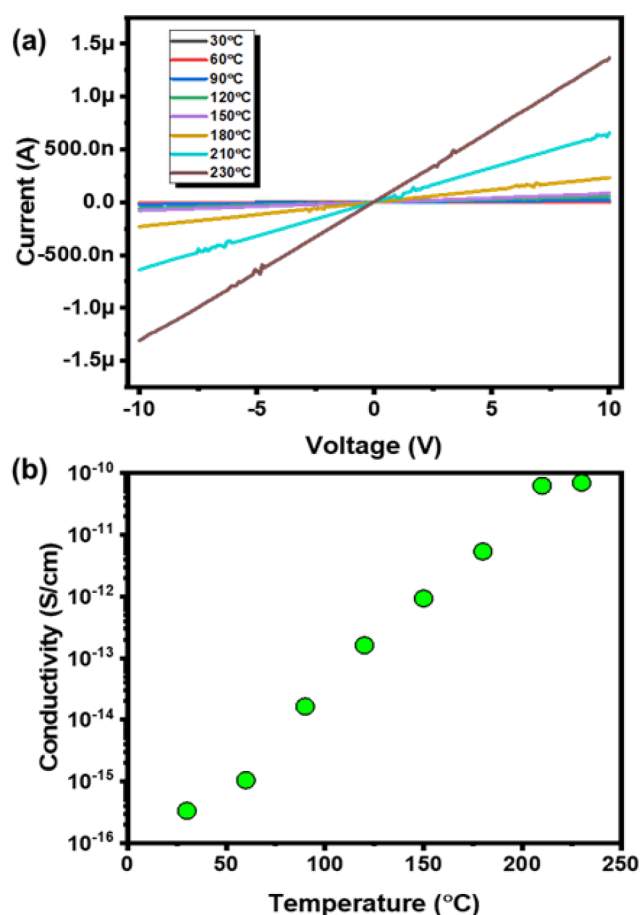
Figure 4. Two-terminal electrical characterization of the crystal: (a) temperature-dependent $I-V$ characteristics; (b) increasing conductivity of $(EDA)CuCl_4$ with temperature.

in conductivity with high stability indicates the potential applicability of this 2D HP crystal in thermal sensors, smart windows, and visual thermometers.

Electronic Band Structure. Since strong ferromagnetic interactions are reported in the literature for the hybrids, the different magnetic state configurations were considered in the electronic structure calculations, as shown in Figure S5a−c. By calculating the total energy in different spin configurations given in Table 1, it is found that the antiferromagnetic configuration type C reaches a stable ground state competing with the ferromagnetic state with slightly lower energy (around 0.159 eV), suggesting strong ferromagnetic interactions in the crystal.

The band structure shows that, near the Fermi energy, the electronic states for both the upward and downward spin channels of the antiferromagnetic (AFM) and ferromagnetic (FM) states are dominated by Cu d and Cl p orbitals (Figure 5, parts a and b), which contribute to the valence band from −1 to −2 eV. In contrast, the minima of the conduction band are influenced by the Cu p and Cl p orbitals. In addition, the C p and N p orbitals also contribute to the low range of the conduction band. EDA is thus found to be semi-semi-conducting with a band gap of 3.4 eV, which is lower than the calculated band gap of 3.70 eV from the Kubelka−Munk function (Figure S3), explained by the usual rules of DFT calculations. The band structure for the stable AFM state is shown in Figure 5c.

Magnetism. Figure 6 shows the temperature dependence of the magnetic susceptibility χ with zero-field cooling (ZFC) and field cooling (FC) in a 1000 Oe magnetic field, $\chi = M/H$, for fields parallel to the crystallographic a-axis or the $(h,0,0)$ plane of the single crystal and for the powdered crystal of $(EDA)CuCl_4$. All curves indicate long-range antiferromagnetic ordering below about 34 K. The temperature dependence of the reciprocal susceptibility $1/\chi$ for the powdered crystal is shown in Figure 6. The paramagnetic (PM) state with a high T value between $T = 150$ and 300 K is well-defined by the Curie−Weiss law $-\chi(T) \sim C/(T - \theta)$, where C is the Curie constant and θ is the paramagnetic Curie constant.[57] The determined effective magnetic moment, μ_{eff}, is 1.727 μB per Cu^{2+}, which corresponds to the pure spin value of $\mu_{calc} = 1.73$ μB for $S = ^1/_2$,[58] suggesting a fully quenched orbital contribution. The fit yields $C = 0.373$ cm^3 K/mol and a positive Weiss temperature of $\theta = 34.47$ K, confirming the presence of FM interactions between the spin states in the PM region with high T,[59] which is also evident from the competing stable AFM and FM states from the electronic structure determination. The basic results for the preliminary magnetic results of the EDA single crystal are consistent with previous reports[34,35] and also confirm the reliability of our forthcoming results. The heat capacity (C_p) measured without a magnetic field is shown in Figure S6a. A thermal anomaly is observed at about 32 K, confirming that it is due to the transition to the magnetic phase, where a similar anomaly is also observed for the C_p at magnetic fields of 1 and 3 T, as shown in Figure S6b. When C_p/T^3 is plotted against T (inset in Figure S6b), a clear peak is seen near the transition temperature, suggesting spin−lattice coupling at this magnetic transition.

The isothermal magnetization curves for the $(EDA)CuCl_4$ crystal recorded in parallel with the magnetic field between 6 and 50 K are shown in Figure 7. The temperature was increased by 4 K from 6 to 30 K. From 30 K, the temperature was increased by 2 K up to 50 K. The field sweep rate is 40 Oe/s. Below T_N, the magnetization makes a jump at a critical field $H_c \sim 10$ kOe. The jump is due to the first-order field-induced metamagnetic transition (FOMT)[60] or spin−flop transitions (this is shown by the derivative of dM/dH as a function of temperature in the figure). Above T_N, H_c disappears and announces the entry of the crystal into the PM state.

The M^2 versus H/M plots, also called a Arrott plots,[61] converted from the measured $M-H$ isotherms are shown in Figure 8a. If the Arrot plot has a positive slope, the magnetic transition is second order; otherwise, a negative slope advocates the transition to be first order. The features of interest in this figure can be summarized as follows: (i) above 36 K, the curves are almost straight upward, showing PM

Table 1. Computed Total Energy by DFT

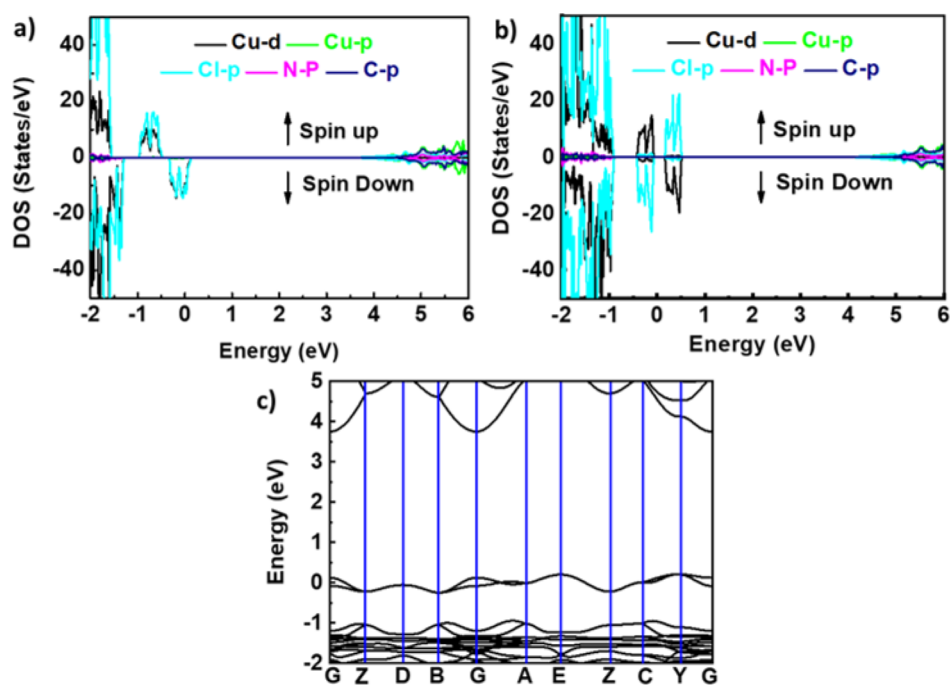| conditions	NM	FM	AFM-A	AFM-C
total energy (eV)	−7293.96288	−7296.85968	−7293.96424	−7297.0188
moment (μ_B)	0.00	7.95	0.00	0.00

Figure 5. Spin-polarized electronic density of states of EDA considering (a) C-type antiferromagnetic and (b) ferromagnetic ordering. (c) Band structure of EDA with C-type antiferromagnetic ordering.
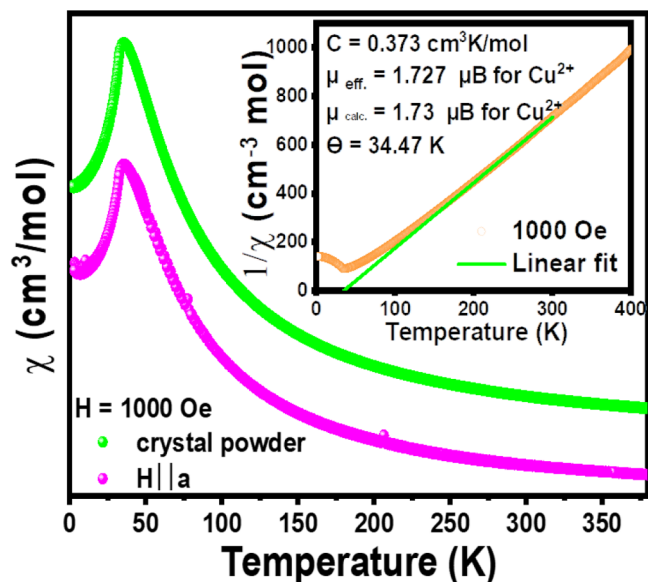

Figure 6. Susceptibility vs temperature for the powder and the single crystal oriented parallel to the magnetic field (a-axis); inset, Curie−Weiss fitting.

Figure 7. Magnetization as a function of the field for the $(EDA)CuCl_4$ SC for temperatures near and below T_N; the derivatives are shown in the inset.

behavior, (ii) below 36 K all the curves show a curvature showing a magnetic behavior, and (iii) with increasing temperatures in the range of 6 K ≤ T ≤ 22 K, the plots are displaced to the right. For T > 22 K, as the temperature is increased, the plots start getting displaced to the left up to 36 K. A clear negative slope at all temperatures below 36 K and direction changes in the Arrott plot indicate one FOMT taking place with a magnetic field for our crystal at about 22 K and another AFM−PM (FM) transition about 36 K. The absence of any type of hysteresis around T_N specifies a reversible MCE exhibited by the $(EDA)CuCl_4$ crystal in magnetic refrigeration applications. The temperature dependence of the change in
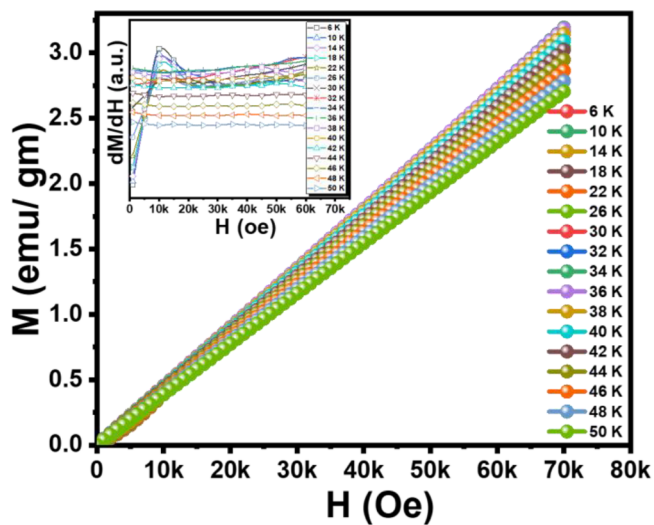
magnetic entropy in an isothermal magnetization process can be calculated by

$$|\Delta S_H| = \sum_i \frac{M_i - M_{i+1}}{T_{i+1} - T_i} \Delta H_i \tag{1}$$

where M_i and M_{i+1} are the experimental values of the magnetization at T_i and T_{i+1} (temperature), respectively, under an applied magnetic field H_i.[49,62]

The entropy changes (ΔS_m) associated with magnetic field variations have been calculated with eq 1, and the temperature dependence of $-\Delta S_m$ for different magnetic fields is shown in Figure 7. The ΔS_m versus T MCE curve is a combination of IMCE and CMCE, which is occasionally reported in the literature in other hosts[45,63] but also reported the first time for
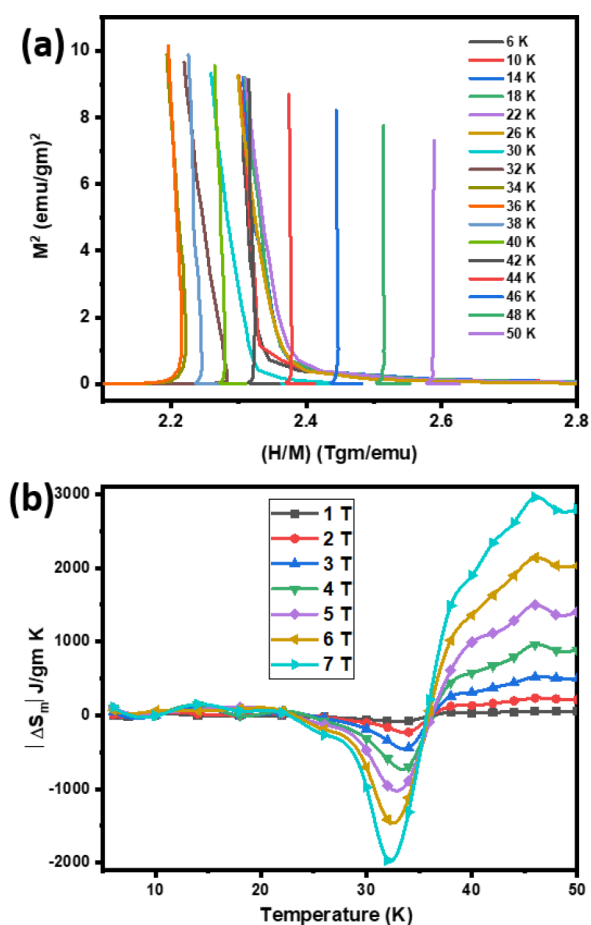
Figure 8. (a) Arrott plot and (b) change in entropy vs temperature curves for the $(EDA)CuCl_4$ SC.

any perovskite host. IMCEs are more common for antiferromagnetic compounds and often observed in systems displaying FOMTs.[64−66] From the ΔS_m versus T curve, it is observed that at lower temperatures up to 22 K the value of ΔS_m remains constant, almost close to 0. Then, above 22 K, the values change sign exhibiting a large positive maximum or IMCE at 34 K, which corresponds to the principal antiferromagnetic transition. The transition happening at 22 K can be ascribed to the FOMT from one AFM state to another AFM state as discussed before. The positive entropy changes for the field changes in the range of 1−7 T. A positive value of ΔS_m increases with an increase in the magnetic field, meaning no increase in configurational magnetic entropy, and it reaches a maximum of 1.97 J kg^{-1} K^{-1} for the magnetic field change of 0−7 T around the transition temperature.

Above 35 K, ΔS_m changes sign to a value of −2.9 J kg^{-1} K^{-1} for magnetic field changes of 7 T reflecting an apparent predictable paramagnetic change in entropy with the applied field. But in our case, this transition or the CMCE can be associated with the AFM/FM transition due to the presence of strong FM interactions in the high-temperature PM region as already proved before. The argument behind the observed feature is that at a lower temperature below 22 K and above 35 K the spin configurations of the Cu atoms in consecutive layers are magnetically more ordered with spins aligned parallel to the magnetic field. However, as the temperature moves to the transition temperature T_N, the applied magnetic field leads to a further spin-disordered state, thus raising the configurational

entropy as IMCE, and hence, the dominating presence of the AFM state is observed. Though the lower temperature spin states remain indifferent to the field, above 22 K the value of the maximum and minimum entropy (ΔS_{max} and ΔS_{min}) change goes on increasing with the increase in the magnetic field indicating the strong dependence of the spin states of the different layers of Cu atoms. The negative ΔS_m even in the presence of the highest magnetic field of 7 T signifies the unquenched antiferromagnetism in the system for high magnetic fields, and the contribution of FM interactions in the PM region increases accordingly, leading to the more ordered spin contribution above T_N. Since materials showing IMCE can find application in heat pumps, the presence of both types of MCE makes this compound suitable for multistage refrigeration,[45] i.e., above 34 K it can work as an active material in the usual working cycle and below that as a reverse working cycle or a heat pump.

CONCLUSIONS

A solution synthesis route followed by slow evaporation was used to synthesize golden-colored crystals of the 2D perovskite $(EDA)CuCl_4$, and their structural, optical, thermal, and magnetic properties were studied. The crystals exhibited a preference for growth along the a-axis with (h00) diffraction peaks. The material is crystallized in a monoclinic space group with $CuCl_4^{2-}$ in the square distorted planar structure. The crystal exhibited reversible thermochromism, high-value temperature-dependent conductivity change, and strong antiferromagnetism with layered ferromagnetic interactions. The reversible thermochromic temperature observed at about 230 °C is due to the sole effect of thermal lattice expansion and is the highest among 2D perovskites ever reported. Magnetic studies have confirmed its antiferromagnetic nature at 34 K. For the first time, detailed experiments for the magnetocaloric effect in this stable 2D inorganic−organic (IO) hybrid system have revealed both inverse and normal MCE. The field-induced MCE conversion under 22 K is related to the FOMT from one AFM state to another, while above T_N, it is due to the interaction between the AFM and FM states. The ΔS_m value increases from a minimum of ∼0.073 J kg^{-1} K^{-1} at a magnetic field change of 0−10 kOe to a maximum of ∼1.97 J kg^{-1} K^{-1} for the magnetic field change in the range of 0−70 kOe. The above features combining thermochromism and MCE suggest that the 2D IO hybrid can be a promising multiapplicable material in a wide range of temperatures. These properties propel this material in the direction of the application of 2D perovskites as smart materials with high stability. Since the layered perovskite $(EDA)CuCl_4$ is eco-friendly, chemically and thermally stable, low-cost, and easy to synthesize, it can be used for low-temperature magnetic refrigeration technology as well as thermal sensors from RT to higher temperatures.

ASSOCIATED CONTENT

ⓢ Supporting Information

The Supporting Information is available free of charge at https://pubs.acs.org/doi/10.1021/acsaelm.1c01108.

> Experimental and simulated XRD of the crystal, refinement and structural parameters of $(EDA)CuCl_4$, TG DSC analysis and temperature variation of the band gap of the single crystal, repeatability and hysteresis curves of the absorption band edge variation with

temperature, different magnetic configurations, and the specific heat capacity study for the single crystal (PDF)

■ AUTHOR INFORMATION

Corresponding Authors

Chun-Wei Chen − *Department of Material Science and Engineering, National Taiwan University, Taipei 10617, Taiwan;* ● orcid.org/0000-0003-3096-249X; Email: chunwei@ntu.edu.tw

Raman Sankar − *Institute of Physics, Academia Sinica, Taipei 11529, Taiwan;* ● orcid.org/0000-0003-4702-2517; Email: sankarndf@gmail.com

Authors

Somrita Dutta − *Department of Material Science and Engineering, National Taiwan University, Taipei 10617, Taiwan; Institute of Physics, Academia Sinica, Taipei 11529, Taiwan*

Deepak Vishnu S. K − *Institute of Physics, Academia Sinica, Taipei 11529, Taiwan; Department of Chemistry, National Tsing Hua University, Hsinchu 300044, Taiwan; NTU−MST International Graduate Program of Molecular Science and Technology, National Taiwan University, Taipei 10617, Taiwan*

Sudipta Som − *Department of Chemical Engineering, National Taiwan University, Taipei 10617, Taiwan;* ● orcid.org/0000-0002-5582-3659

Rajneesh Chaurasiya − *Department of Material Science and Engineering, National Cheng Kung University, Tainan 701, Taiwan;* ● orcid.org/0000-0002-3301-2089

Dinesh Kumar Patel − *Department of Physics, National Taiwan University, Taipei 10617, Taiwan*

Kalimuthu Moovendaran − *Institute of Physics, Academia Sinica, Taipei 11529, Taiwan*

Cheng-Chieh Lin − *NTU−MST International Graduate Program of Molecular Science and Technology, National Taiwan University, Taipei 10617, Taiwan; Molecular Science and Technology Program, Taiwan International Graduate Program, Academia Sinica, Taipei 11529, Taiwan;* ● orcid.org/0000-0003-1895-493X

Complete contact information is available at:
https://pubs.acs.org/10.1021/acsaelm.1c01108

Notes

The authors declare no competing financial interest.

■ REFERENCES

(1) Kojima, A.; Teshima, K.; Shirai, Y.; Miyasaka, T. Organometal Halide Perovskites as Visible-Light Sensitizers for Photovoltaic Cells. *J. Am. Chem. Soc.* **2009**, *131* (17), 6050−6051.

(2) Motta, C.; El-Mellouhi, F.; Sanvito, S. Charge Carrier Mobility in Hybrid Halide Perovskites. *Sci. Rep.* **2015**, *5* (1), 12746.

(3) Yin, W.-J.; Shi, T.; Yan, Y. Unique Properties of Halide Perovskites as Possible Origins of the Superior Solar Cell Performance. *Adv. Mater.* **2014**, *26* (27), 4653−4658.

(4) Smith, M. D.; Crace, E. J.; Jaffe, A.; Karunadasa, H. I. The Diversity of Layered Halide Perovskites. *Annu. Rev. Mater. Res.* **2018**, *48* (1), 111−136.

(5) Cao, D. H.; Stoumpos, C. C.; Farha, O. K.; Hupp, J. T.; Kanatzidis, M. G. 2D Homologous Perovskites as Light-Absorbing Materials for Solar Cell Applications. *J. Am. Chem. Soc.* **2015**, *137* (24), 7843−7850.

(6) Pandey, S.; Andrews, A. P.; Venugopal, A. Manifestation of Helicity in One-Dimensional Iodobismuthate. *Dalt. Trans.* **2016**, *45* (21), 8705−8707.

(7) Sun, C.; Wang, M.-S.; Li, P.-X.; Guo, G.-C. Conductance Switch of a Bromoplumbate Bistable Semiconductor by Electron-Transfer Thermochromism. *Angew. Chemie Int. Ed.* **2017**, *56* (2), 554−558.

(8) Wan, K.-M.; Tong, Y.-B.; Li-Li; Zou, Y.; Duan, H.-B.; Liu, J.-L.; Ren, X.-M. Investigation of Thermochromic Photoluminescent, Dielectric, and Crystal Structural Properties for an Inorganic−Organic Hybrid Solid of [1-Hexyl-3-Methylimidazolium][PbBr$_3$]. *New J. Chem.* **2016**, *40* (10), 8664−8672.

(9) Novoselov, K. S.; Geim, A. K.; Morozov, S. V.; Jiang, D.; Zhang, Y.; Dubonos, S. V.; Grigorieva, I. V.; Firsov, A. A. Electric Field Effect in Atomically Thin Carbon Films. *Science (80-.)* **2004**, *306* (5696), 666−669.

(10) Mak, K. F.; Lee, C.; Hone, J.; Shan, J.; Heinz, T. F. Atomically Thin MoS$_2$: A New Direct-Gap Semiconductor. *Phys. Rev. Lett.* **2010**, *105* (13), 136805.

(11) Allen, M. J.; Tung, V. C.; Kaner, R. B. Honeycomb Carbon: A Review of Graphene. *Chem. Rev.* **2010**, *110* (1), 132−145.

(12) Bella, F.; Griffini, G.; Correa-Baena, J.-P.; Saracco, G.; Gratzel, M.; Hagfeldt, A.; Turri, S.; Gerbaldi, C. Improving Efficiency and Stability of Perovskite Solar Cells with Photocurable Fluoropolymers. *Scienc* **2016**, *354* (6309), 203−206.

(13) Eperon, G. E.; Leijtens, T.; Bush, K. A.; Prasanna, R.; Green, T.; Wang, J. T.-W.; McMeekin, D. P.; Volonakis, G.; Milot, R. L.; May, R.; et al. Perovskite-Perovskite Tandem Photovoltaics with Optimized Band Gaps. *Science* **2016**, *354* (6314), 861−865.

(14) Li, J.; Xu, C.; Zhang, W.-Y.; Shi, P.-P.; Ye, Q.; Fu, D.-W. Smart and Efficient Opto-Electronic Dual Response Material Based on Two-Dimensional Perovskite Crystal/Thin Film. *J. Mater. Chem. C* **2020**, *8* (6), 1953−1961.

(15) Saparov, B.; Mitzi, D. B. Organic-Inorganic Perovskites: Structural Versatility for Functional Materials Design. *Chem. Rev.* **2016**, *116* (7), 4558−4596.

(16) Stoumpos, C. C.; Cao, D. H.; Clark, D. J.; Young, J.; Rondinelli, J. M.; Jang, J. I.; Hupp, J. T.; Kanatzidis, M. G. Ruddlesden−Popper Hybrid Lead Iodide Perovskite 2D Homologous Semiconductors. *Chem. Mater.* **2016**, *28* (8), 2852−2867.

(17) Pan, Y.; Wang, H.; Li, X.; Zhang, X.; Liu, F.; Peng, M.; Shi, Z.; Li, C.; Zhang, H.; Weng, Z.; Gusain, M.; Long, H.; Li, D.; Wang, J.; Zhan, Y.; Zheng, L. Detection Range Extended 2D Ruddlesden−Popper Perovskite Photodetectors. *J. Mater. Chem. C* **2020**, *8* (10), 3359−3366.

(18) Raghavan, C. M.; Chen, T.-P.; Li, S.-S.; Chen, W.-L.; Lo, C.-Y.; Liao, Y.-M.; Haider, G.; Lin, C.-C.; Chen, C.-C.; Sankar, R.; Chang, Y.-M.; Chou, F.-C.; Chen, C.-W. Low-Threshold Lasing from 2D Homologous Organic-Inorganic Hybrid Ruddlesden−Popper Perovskite Single Crystals. *Nano Lett.* **2018**, *18* (5), 3221−3228.

(19) Chatterjee, S.; Pal, A. J. Influence of Metal Substitution on Hybrid Halide Perovskites: Towards Lead-Free Perovskite Solar Cells. *J. Mater. Chem. A* **2018**, *6* (9), 3793−3823.

(20) Zimmermann, I.; Aghazada, S.; Nazeeruddin, M. K. Lead and HTM Free Stable Two-Dimensional Tin Perovskites with Suitable Band Gap for Solar Cell Applications. *Angew. Chemie Int. Ed.* **2019**, *58* (4), 1072−1076.

(21) Ma, L.; Ju, M.-G.; Dai, J.; Zeng, X. C. Tin, and Germanium Based Two-Dimensional Ruddlesden−Popper Hybrid Perovskites for Potential Lead-Free Photovoltaic and Photoelectronic Applications. *Nanoscale* **2018**, *10* (24), 11314−11319.

(22) Butler, E. Book Review: N. N. Greenwood, A. Earnshaw: Chemistry of the elements. Pergamon press oxford 1984, 1542 seiten,

7 anhänge Preis: US $ 34.95. ISBN 0−08−022057−6. *Cryst. Res. Technol.* **1985**, *20* (5), 662.

(23) Khomskii, D. I.; Kugel, K. I. Orbital and Magnetic Structure of Two-Dimensional Ferromagnets with Jahn-Teller Ions. *Solid State Commun.* **1973**, *13* (7), 763−766.

(24) Polyakov, A. O.; Arkenbout, A. H.; Baas, J.; Blake, G. R.; Meetsma, A.; Caretta, A.; van Loosdrecht, P. H. M.; Palstra, T. T. M. Coexisting Ferromagnetic and Ferroelectric Order in a CuCl^{+}Based Organic-Inorganic Hybrid. *Chem. Mater.* **2012**, *24* (1), 133−139.

(25) de Jongh, L. J. Experiments on Simple Magnetic Model Systems. *J. Appl. Phys.* **1978**, *49* (3), 1305−1310.

(26) Nafday, D.; Sen, D.; Kaushal, N.; Mukherjee, A.; Saha-Dasgupta, T. 2D Ferromagnetism in Layered Inorganic-Organic Hybrid Perovskites. *Phys. Rev. Res.* **2019**, *1* (3), 32034.

(27) Monroe, J. C.; Carvajal, M. A.; Deumal, M.; Landee, C. P.; Rademeyer, M.; Turnbull, M. M. Revisiting the Role of Hydrogen Bonding in the Strong Dimer Superexchange of a 2D Copper(II) Halide Honeycomb-Like Lattice: Structural and Magnetic Study. *Inorg. Chem.* **2020**, *59* (9), 6319−6331.

(28) Abdel-Aal, S. K.; Abdel-Rahman, A. S. Fascinating Physical Properties of 2D Hybrid Perovskite $[(NH_3)(CH_2)_7(NH_3)]$-CuCl$_x$Br$_{4-x}$, x = 0, 2 and 4. *J. Electron. Mater.* **2019**, *48* (3), 1686−1693.

(29) Cortecchia, D.; Dewi, H. A.; Yin, J.; Bruno, A.; Chen, S.; Baikie, T.; Boix, P. P.; Grätzel, M.; Mhaisalkar, S.; Soci, C.; Mathews, N. Lead-Free MA$_2$CuCl$_x$Br$_{4−x}$ Hybrid Perovskites. *Inorg. Chem.* **2016**, *55* (3), 1044−1052.

(30) Elseman, A. M.; Shalan, A. E.; Sajid, S.; Rashad, M. M.; Hassan, A. M.; Li, M. Copper-Substituted Lead Perovskite Materials Constructed with Different Halides for Working (CH$_3$NH$_3$)$_2$CuX$_4$-Based Perovskite Solar Cells from Experimental and Theoretical View. *ACS Appl. Mater. Interfaces* **2018**, *10* (14), 11699−11707.

(31) Li, J.; Liu, X.; Cui, P.; Li, J.; Ye, T.; Wang, X.; Zhang, C.; Zhao, Y. S. Lead-Free Thermochromic Perovskites with Tunable Transition Temperatures for Smart Window Applications. *Sci. China Chem.* **2019**, *62* (9), 1257−1262.

(32) Pandey, P.; Sharma, N.; Panchal, R. A.; Gosavi, S. W.; Ogale, S. Realization of High Capacity and Cycling Stability in Pb-Free A$_2$CuBr$_4$ (A = CH$_3$NH$_3$/Cs, 2 D/3 D) Perovskite-Based Li-Ion Battery Anodes. *ChemSusChem* **2019**, *12* (16), 3742−3746.

(33) Birrell, G. B.; Zaslow, B. The Crystal Structure of (NH$_3$CH$_2$CH$_2$NH$_3$)(CuCl$_4$). *J. Inorg. Nucl. Chem.* **1972**, *34* (5), 1751.

(34) Tichý, K.; Beneš, J.; Hälg, W.; Arend, H. Neutron Diffraction Study of Twinned Crystals of Ethylenediammonium Copper Tetrachloride and Ethylenediammonium Manganese Tetrachloride. *Acta Crystallogr. Sect. B Struct. Crystallogr. Cryst. Chem.* **1978**, *34* (10), 2970−2981.

(35) von Känel, H. Magnetic and Optical Properties of the Layer Type Magnets (CH$_2$)$_2$(ND$_3$)$_2$MnCl$_4$ and (CH$_2$)$_n$(NH$_3$)$_2$CuCl$_4$, n = 2, 3, 5. *Physica B+C* **1979**, *96* (2), 167−193.

(36) Snively, L. O.; Seifert, P. L.; Emerson, K.; Drumheller, J. E. Magnetic Susceptibility of (NH$_3$CH$_2$CH$_2$NH$_3$)CuCl$_4$: A Layered Structure with Strong Interlayer Magnetic Coupling. *Phys. Rev. B* **1979**, *20* (5), 2101−2104.

(37) Iqbal, Z.; Arend, H.; Wachter, P. Raman Scattering from Layer-Type Magnets: (CH$_2$)$_n$(NH$_3$)$_2$CuCl$_4$, N = 2, 3 and 5. *J. Phys. C Solid State Phys.* **1980**, *13* (25), 4757−4767.

(38) Snively, L. O.; Tuthill, G. F.; Drumheller, J. E. Measurement and Calculation of the Superexchange Interaction through the Two-Halide Bridge in the Eclipsed Layered Compounds [NH$_3$(CH$_2$)$_n$NH$_3$]CuX for n = 2−5 and X = Cl$_4$ and Cl$_2$Br$_2$ An. *Phys. Rev. B* **1981**, *24* (9), 5349−5355.

(39) Abdel-Aal, S. K.; Kocher-Oberlehner, G.; Ionov, A.; Mozhchil, R. N. Effect of organic chain length on structure, electronic composition, lattice potential energy, and optical properties of 2D hybrid perovskites [(NH$_3$)(CH$_2$)$_n$(NH$_3$)]CuCl$_4$, n = 2−9. *Appl. Phys. A: Mater. Sci. Process.* **2017**, *123*, 531.

(40) Lim, A. R. Dynamics of NH$_3$(CH$_2$)$_2$NH$_3$ Cation in Perovskite Layer Crystal NH$_3$(CH$_2$)$_2$NH$_3$CuCl$_4$ by M. *Solid State Commun.* **2020**, *312*, 113862.

(41) Choi, S.; Larrabee, J. A. Thermochromic Tetrachlorocuprate-(II): An Advanced Integrated Laboratory Experiment. *J. Chem. Educ.* **1989**, *66* (9), 774.

(42) Conings, B.; Drijkoningen, J.; Gauquelin, N.; Babayigit, A.; D'Haen, J.; D'Olieslaeger, L.; Ethirajan, A.; Verbeeck, J.; Manca, J.; Mosconi, E.; Angelis, F. De; Boyen, H.-G. Intrinsic Thermal Instability of Methylammonium Lead Trihalide Perovskite. *Adv. Energy Mater.* **2015**, *5* (15), 1500477.

(43) GschneidnerJr, K. A.; Pecharsky, V. K.; Tsokol, A. O. Recent Developments in Magnetocaloric Materials. *Rep. Prog. Phys.* **2005**, *68* (6), 1479−1539.

(44) Glanz, J. Making a Bigger Chill With Magnets. *Science (80-.).* **1998**, *279* (5359), 2045.

(45) Shen, B. G.; Sun, J. R.; Hu, F. X.; Zhang, H. W.; Cheng, Z. H. Recent Progress in Exploring Magnetocaloric Materials. *Adv. Mater.* **2009**, *21* (45), 4545−4564.

(46) Zheng, X. Q.; Xu, Z. Y.; Zhang, B.; Hu, F. X.; Shen, B. G. The Normal and Inverse Magnetocaloric Effect in RCu$_2$ (R = Tb, Dy, Ho, Er) Compounds. *J. Magn. Magn. Mater.* **2017**, *421*, 448−452.

(47) Krenke, T.; Duman, E.; Acet, M.; Wassermann, E. F.; Moya, X.; Mañosa, L.; Planes, A. Inverse Magnetocaloric Effect in Ferromagnetic Ni−Mn−Sn Alloys. *Nat. Mater.* **2005**, *4* (6), 450−454.

(48) Sen, A.; Roy, S.; Peter, S. C.; Paul, A.; Waghmare, U. V.; Sundaresan, A. Order-Disorder Structural Phase Transition and Magnetocaloric Effect in Organic-Inorganic Halide Hybrid (C$_2$H$_5$NH$_3$)$_2$CoCl$_4$. *J. Solid State Chem.* **2018**, *258*, 431−440.

(49) Ma, Y.; Zhai, K.; Yan, L.; Chai, Y.; Shang, D.; Sun, Y. Magnetocaloric Effect in the Layered Organic-Inorganic Hybrid (CH3NH3)2CuCl4. *Chin. Phys. B* **2018**, *27*, 027501.

(50) Bochalya, M.; Kumar, S. Magnetocaloric Effect in 2D-Alkylammonium Copper Halides Layered Inorganic-Organic Systems. *J. Appl. Phys.* **2020**, *127* (5), 055501.

(51) Giannozzi, P.; Baroni, S.; Bonini, N.; Calandra, M.; Car, R.; Cavazzoni, C.; Ceresoli, D.; Chiarotti, G. L.; Cococcioni, M.; Dabo, I.; Dal Corso, A.; de Gironcoli, S.; Fabris, S.; Fratesi, G.; Gebauer, R.; Gerstmann, U.; Gougoussis, C.; Kokalj, A.; Lazzeri, M.; Martin-Samos, L.; Marzari, N.; Mauri, F.; Mazzarello, R.; Paolini, S.; Pasquarello, A.; Paulatto, L.; Sbraccia, C.; Scandolo, S.; Sclauzero, G.; Seitsonen, A. P.; Smogunov, A.; Umari, P.; Wentzcovitch, R. M. QUANTUM ESPRESSO: A Modular and Open-Source Software Project for Quantum Simulations of Materials. *J. Phys.: Condens. Matter* **2009**, *21* (39), 395502.

(52) Perdew, J. P.; Burke, K.; Ernzerhof, M. Generalized Gradient Approximation Made Simple. *Phys. Rev. Lett.* **1996**, *77* (18), 3865−3868.

(53) Pack, J. D.; Monkhorst, H. J. Special Points for Brillouin-Zone Integrations"—a Reply. *Phys. Rev. B* **1977**, *16* (4), 1748−1749.

(54) Sun, B.; Liu, X.-F.; Li, X.-Y.; Cao, Y.; Yan, Z.; Fu, L.; Tang, N.; Wang, Q.; Shao, X.; Yang, D.; Zhang, H.-L. Reversible Thermochromism and Strong Ferromagnetism in Two-Dimensional Hybrid Perovskites. *Angew. Chemie Int. Ed.* **2020**, *59* (1), 203−208.

(55) Elattar, A.; Suzuki, H.; Mishima, R.; Nakao, K.; Ota, H.; Nishikawa, T.; Inoue, H.; Kyaw, A. K. K.; Hayashi, Y. Single Crystal of Two-Dimensional Mixed-Halide Copper-Based Perovskites with Reversible Thermochromism. *J. Mater. Chem. C* **2021**, *9* (9), 3264−3270.

(56) Singh, A.; Satapathi, S. Reversible Thermochromism in All-Inorganic Lead-Free Cs$_3$Sb$_2$I$_9$ Perovskite Single Crystals. *Adv. Opt. Mater.* **2021**, *9* (22), 2101062.

(57) Panneer Muthuselvam, I.; Saranya, K.; Büscher, F.; Wulferding, D.; Lemmens, P.; Chen, W.; Sankar, R. High Magnetic Anisotropy and Magnon Excitations in Single Crystals of the Double Spin Chain Compound PbMn$_2$Ni$_6$Te$_3$O$_{18}$. *Phys. Rev. B* **2021**, *103* (6), 64401.

(58) Murugan, G. S.; Chen, P. J.; Sankar, R.; Muthuselvam, I. P.; Rao, G. N.; Chou, F. C. Antiferromagnetism of Li$_2$Cu$_5$Si$_4$O$_{14}$ with

Alternating Dimers and Trimers in Chains. *Phys. Rev. B* **2017**, *95* (17), 174442.

(59) Samanta, T.; Das, I.; Banerjee, S. Comparative Studies of Magnetocaloric Effect and Magnetotransport Behavior in GdRu$_2$Si$_2$ Compound. *J. Appl. Phys.* **2008**, *104* (12), 123901.

(60) Dong, Q. Y.; Hou, K. Y.; Zhang, X. Q.; Su, L.; Wang, L. C.; Ke, Y. J.; Yan, H. T.; Cheng, Z. H. Giant Reversible Magnetocaloric Effect in Antiferromagnetic Rare-Earth Cobaltite GdCoO$_3$. *J. Appl. Phys.* **2020**, *127* (3), 033904.

(61) Mondal, S.; Midya, A.; Patidar, M. M.; Ganesan, V.; Mandal, P. Magnetic and Magnetocaloric Properties of Layered van Der Waals CrCl$_3$. *Appl. Phys. Lett.* **2020**, *117* (9), 092405.
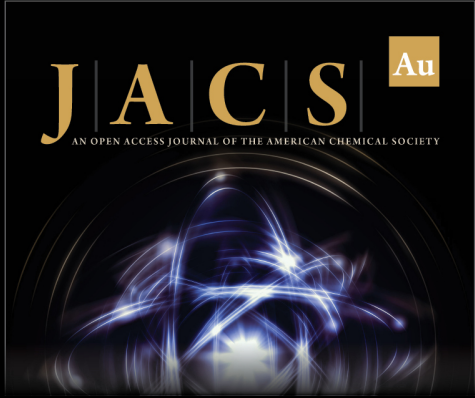
(62) Shen, J.; Zhao, J.-L.; Hu, F.-X.; Rao, G.-H.; Liu, G.-Y.; Wu, J.-F.; Li, Y.-X.; Sun, J.-R.; Shen, B.-G. Magnetocaloric Effect in Antiferromagnetic Dy$_3$Co Compound. *Appl. Phys. A: Mater. Sci. Process.* **2010**, *99* (4), 853−858.

(63) Zhang, Q.; Guillou, F.; Wahl, A.; Bréard, Y.; Hardy, V. Coexistence of Inverse and Normal Magnetocaloric Effect in A-Site Ordered NdBaMn$_2$O$_6$. *Appl. Phys. Lett.* **2010**, *96* (24), 242506.

(64) Biswas, A.; Chandra, S.; Samanta, T.; Phan, M. H.; Das, I.; Srikanth, H. The Universal Behavior of Inverse Magnetocaloric Effect in Antiferromagnetic Materials. *J. Appl. Phys.* **2013**, *113* (17), 17A902.

(65) Gottschilch, M.; Gourdon, O.; Persson, J.; de la Cruz, C.; Petricek, V.; Brueckel, T. Study of the Antiferromagnetism of Mn$_5$Si$_3$: An Inverse Magnetocaloric Effect Material. *J. Mater. Chem.* **2012**, *22* (30), 15275−15284.

(66) Hu, W. J.; Du, J.; Li, B.; Zhang, Q.; Zhang, Z. D. Giant Magnetocaloric Effect in the Ising Antiferromagnet DySb. *Appl. Phys. Lett.* **2008**, *92* (19), 192505.